Temperature dependence of shot noise in double barrier magnetic tunnel junctions

Jiasen Niu, Liang Liu, J. F. Feng, X. F. Han, J. M. D. Coey, X.-G. Zhang, and Jian Wei

Temperature dependence of shot noise in double barrier magnetic tunnel junctions

Jiasen Niu,[1, 2, *] Liang Liu,[1, 2] J. F. Feng,[3, 4] X. F. Han,[3, 4] J. M. D. Coey,[5] X.-G. Zhang,[6] and Jian Wei[1, 2]

[1]*International Center for Quantum Materials, School of Physics, Peking University, Beijing 100871, China*
[2]*Collaborative Innovation Center of Quantum Matter, Beijing, China*
[3]*Beijing National Laboratory of Condensed Matter Physics,*
Institute of Physics, Chinese Academy of Sciences, Beijing 100190, China
[4]*University of Chinese Academy of Sciences, Beijing 100049, China*
[5]*CRANN and School of Physics, Trinity College, Dublin 2, Ireland*
[6]*Department of Physics and the Quantum Theory Project, University of Florida, Gainesville 32611, USA*
(Dated: February 28, 2018)

Shot noise reveals spin dependent transport properties in a magnetic tunnel junction(MTJ). We report measurement of shot noise in CoFeB/MgO/CoFeB/MgO/CoFeB double barrier magnetic tunnel junctions(DBMTJs), which shows a strong temperature dependence. The Fano factor used to characterise shot noise increases with decreasing temperature. A sequential tunneling model can be used to account for these results, in which a larger Fano factor results from larger spin relaxation length at lower temperatures.

I. INTRODUCTION

Magnetic tunnel junctions(MTJs)[1,2] have broad application prospects due to their giant tunneling magnetoresistance(TMR)[3–9]. MTJs based on symmetry-preserved tunneling have been used for read heads of hard disk drives and data storage such as STT-MRAM[10]. Double barrier magnetic tunnel junctions(DBMTJs) have potential advantages over single barrier magnetic tunnel junctions(SBMTJs) due to their better signal to noise ratio[11–15]. DBMTJ can generate a larger output voltage at the relevant operating voltage, which can improve the signal to noise ratio[16,17].

Shot noise is a powerful tool for studying spin dependent tunneling processes in MTJs[18–23] It reveals the discrete nature of electrons and can be characterised by Fano factor(F). In the zero temperature limit, the Fano factor is defined $F = \frac{S_I}{2eI}$, where S_I is the experimental current noise power. If electrons tunnel through the barrier independently (Poissonian process), $F = 1$ which means full shot noise[24]. Full shot noise has been measured in SBMTJs with large TMR[18,22,25]. It is usually suppressed ($F < 1$) in DBMTJs due to two step tunneling[19]. Magnetic control of shot noise was reported recently in weakly asymmetric epitaxial Fe/MgO/Fe/MgO/Fe DBMTJs[20,26]. However, in previous reports shot noise in DBMTJs was measured below 10 K to avoid the influence of 1/f noise[20,22]. Measurement of shot noise at higher temperatures and further study of the variation of shot noise at different temperatures are helpful for potential applications at room temperature as well as for understanding spin relaxations in DBMTJs.

In this work, we develop a high-frequency noise measurement setup and successfully measure shot noise in a large temperature range from 296 K to 20 K. We find that shot noise can be tuned not only by magnetic states but also by temperature in sputtered DBMTJs. The Fano factor increases significantly as temperature decreases from 296 K to 20 K. A sequential tunneling model with
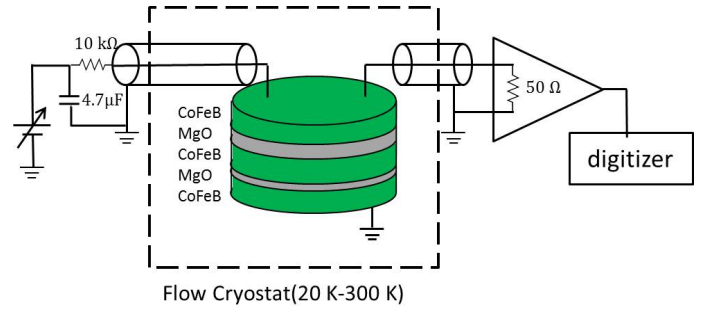

FIG. 1. (color online) Schematic of measurement setup and device structure. The left side shows the DC bias circuit and the right side shows the noise signal acquisition circuit.

consideration of spin relaxation[20] is used to explain our results.

II. METHOD:HIGH FREQUENCY MEASUREMENT SETUP

It is difficult to measure shot noise at high temperature due to large 1/f noise in DBMTJs and low frequency bandwidth normally used. Although we can try to measure shot noise with a large bias current, 1/f noise increases much more quickly than shot noise with increasing bias especially at high temperatures[27,28]. So it is necessary to measure shot noise at high frequency in order to minimize the influence of 1/f noise. To reach high frequency, we use a high frequency amplifier(MITEQ AU-1447) and high frequency SMA connector. The AU-1447 has an input impedance of 50Ω, and is used to measure current noise from device. Figure 1 shows the schematic diagram of our noise measurement setup. At the left side, we use a digital voltage source Agilent B2901A decoupled by a home-made battery-powered optical decoupler circuit and a RC filter as a low noise current source. At the right side, the noise from the device is amplified with the
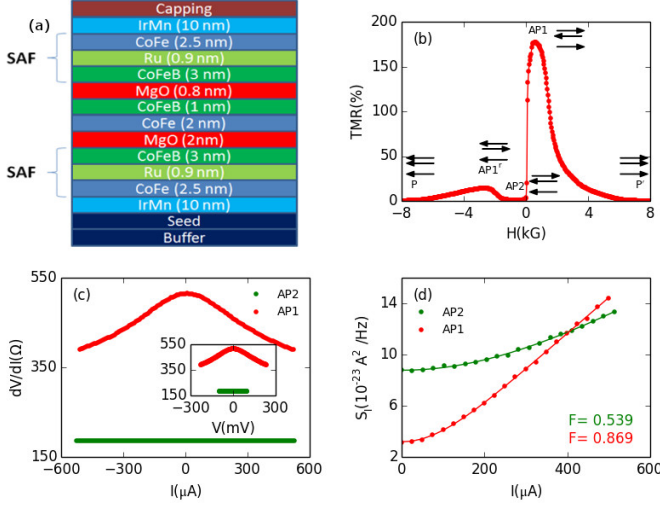
FIG. 2. (color online) (a)Schematic diagram of the stack of asymmetric DBMTJ. (b)TMR for our sample at room temperature. (c)Differential resistance of AP1 (red) and AP2 (green) states at room temperature, which is needed to calculate the current noise power fitting line. The insert shows the voltage dependence of resistance. (d)Bias dependence of current noise power S_I at room temperature of AP1 and AP2 states. The red and green dots are experimental data and solid lines are noise fitting lines from which we estimate the F by using Eq.1. The intercept is thermal noise. The F is smaller than 1 for both states.
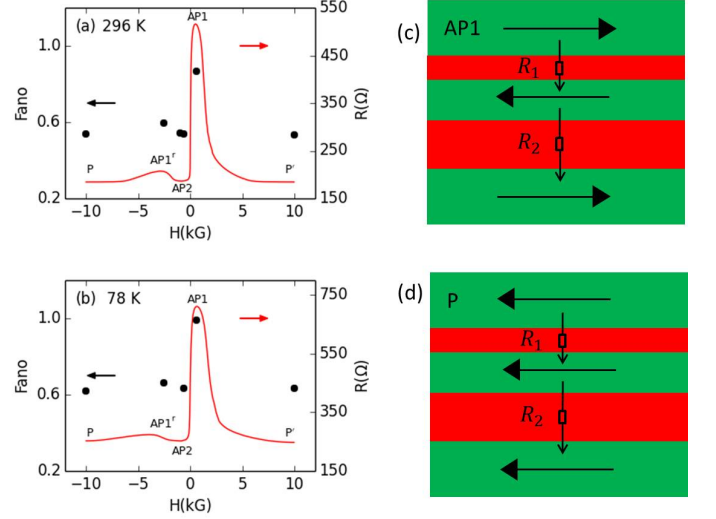

FIG. 3. (color online) Field dependence of F at 296 K(a) and 78 K (b). Red solid lines are MR curves and black dots are F. For both temperatures, F shows magnetic state dependence. The Fano factor for the AP1 state is much larger than for the others. (c) and (d) show the magnetization orientation of AP1 and P state. At AP1 state, R_2 is much larger than R_1, which leads to a larger F than in the P state where R_2 is comparable to R_1.

AU-1447 and then digitized by a data acquisition card.

Current noise of sample is measured in the range of 2.1-2.5 MHz, within which 1/f noise is ten times smaller than shot noise even at room temperature. A typical noise spectrum is shown in Appendix A.

III. RESULTS AND DISCUSSION

A. Device and shot noise fitting

Figure 2(a) shows a simple schematic of a DBMTJ stack with two synthetic anti-ferromagnetic layers(SAF), two asymmetric MgO barriers and a free layer in between. Sample fabrication was already reported[14]. Figure 2(b) shows the TMR curve at room temperature. There are two different high-resistance states: AP1 ($\downarrow\uparrow\downarrow$) and $AP1^r$ ($\uparrow\downarrow\uparrow$) and three low-resistance states:AP2 ($\downarrow\uparrow\uparrow$),P ($\uparrow\uparrow\uparrow$) and P' ($\downarrow\downarrow\downarrow$)[28].

At finite temperature, white noise power(S_{white}) is given by[24]

$$S_I = \frac{4kT}{R_d} + 2F[eI \coth \frac{eV}{2kT} - \frac{2kT}{R_d}], \qquad (1)$$

where I is the average current, V is the junction voltage, e is the electron charge, k is the Boltzmann constant, T is temperature, R_d is the differential resistance of the junction and F is the Fano factor which is generally independent of temperature. Figure 2(c) and insert show

differential resistance of the AP1 and AP2 states at room temperature, which are used for fitting the shot noise in Fig. 2(d) by using Eq.1. Figure 2(d) shows the current dependence of current noise power S_I for AP1 and AP2 states at room temperature. The dots are experimental data and solid lines are fits to Eq.1. We take into account the thermal noise and use Eq.1 to obtain F. It's obvious that F is less than 1.

B. Magnetic state dependence

It is observed that in sputtered, strongly-asymmetric DBMTJs the Fano factor can be tuned by magnetic states, as shown in Fig. 3(a) and (b) where F of the different states and the MR curves are summarized at two typical temperatures (296 K and 78 K). Black dots and red solid curves in Fig. 3 show F and MR curves. In AP1, F is much larger than in other states at each temperature. The Fano factors of AP2, P and P' are similar and slightly smaller than $AP1^r$.

In previous work, shot noise in epitaxial DBMTJs was shown to depend strongly on the magnetic configuration, and the symmetry of the two barriers, and a sequential tunneling model was used to explain the magnetic state dependence[19,20,26]. Following their work, we have: $F = 1 - \frac{2R_1R_2}{(R_1+R_2)^2}$ where $R_1(R_2)$ is the resistance of first(second) barrier. Figure 3(c) and (d) show the magnetization orientations in the AP1 and P sates. For AP1, R_2 is much larger than R_1 due to sample's asymmetry,
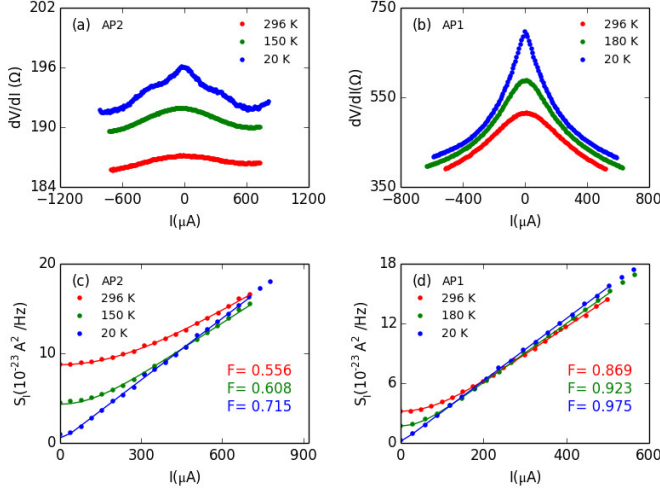
FIG. 4. (color online) Differential resistance and noise power are measured at different temperatures for two states. Differential resistance at different temperatures of AP2 and AP1 states are shown in (a) and (b). In (a), dV/dI changes little with temperature decreasing. In (b), dV/dI increases at low temperatures. Bias dependence of current noise power S_I at different temperatures is measured in (c)AP2 state and (d)AP1 state. From room temperature to low temperature, thermal noise decreases and F increases. As a result, for large bias the noise power at low temperatures is larger than noise power at room temperature.

and F will approach 1, which is similar to the case of a single barrier. While in the P state, R_1 is comparable to R_2, which leads to a lower F than than in AP1 state.

C. Temperature dependence

The Fano factor is usually independent of temperature[24,29]. However, we find that there is a strong temperature dependence in DBMTJs. Figure 4 shows our experimental results at three representative temperatures. Figure 4(c) and (d) show the bias dependence of noise power S_I for AP2 and AP1. For both states F increases and thermal noise decreases from 296 K to 20 K. Figure 4(a) and (b) show the bias dependence of the differential resistance in AP2 and AP1 states. For AP2 states, R_d changes little with temperature especially below 78 K while F changes appreciably. It is obvious that the change of F is not simply related to R_d.

Figure 5(a) summaries the temperature dependence of F for the same two states. In the AP2 state, the Fano factor increases from 0.55 at 296 K to 0.73 at 20 K. While for AP1, F also increases with decreasing temperature and approaches 1 below 78 K.

The temperature dependence in DBMTJs can be explained by sequential tunneling if we take spin into account. Following recent work[20], in the absence of spin relaxation electrons with up spin(spin-up channel) and
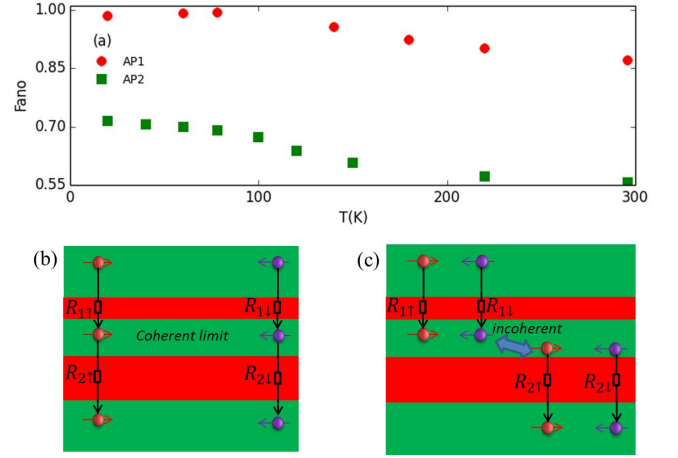

FIG. 5. (color online) (a)Temperature dependence of F for two states(AP1 and AP2). For both states it is much smaller than 1 at room temperature and close to 1 at low temperature for the AP1 state. But for the AP2 state, F continually increases with decreasing temperature. (b)(c)Schematic diagram of two sequential tunneling model (coherent and incoherent limit). Green layers are ferromagnetic and red layers are insulating. (b)At low temperatures, we can ignore spin relaxation in the middle ferromagnetic layer, and the tunneling process can be separated as spin up and spin down channels (coherent limit). These two channels contribute to the total noise power S. (c)When at high temperature, spin relaxation is strong, the tunneling process reaches incoherent limit. It is just like two SBMTJs in series with an island in between them.

electrons with down spin(spin-down channel) tunnel separately. Then for each channel, the noise power is exactly like it is in the case of spinless particles. Therefore shot noise can be calculated as $S = S_\uparrow + S_\downarrow$, where $S_\uparrow$ and $S_\downarrow$ are the contributions from the spin-up and spin-down channels as depicted in Fig. 5(b). In this case F can be expressed as :

$$F_{coherent} = \frac{(R_{1\uparrow}^2 + R_{2\uparrow}^2)R_\downarrow^3 + (R_{1\downarrow}^2 + R_{2\downarrow}^2)R_\uparrow^3}{R_\uparrow^2 R_\downarrow^2 (R_\uparrow + R_\downarrow)}, \quad (2)$$

where $R_{i\sigma}$ is the spin dependent resistance of the i-th(i=1,2) barrier and $R_\sigma = R_{1\sigma} + R_{2\sigma}$. If spin relaxation in the middle layer is strong enough, only charge fluctuations need to be taken into account. In this case, the DBMTJ can be considered as two single barriers in series as shown in Fig. 5(c). Then the F will be

$$F_{incoherent} = \frac{R_{2\uparrow}^2 R_{2\downarrow}^2 (R_{1\uparrow} + R_{1\downarrow})^2 + R_{1\uparrow}^2 R_{1\downarrow}^2 (R_{2\uparrow} + R_{2\downarrow})^2}{[R_{1\uparrow}R_{1\downarrow}(R_{2\uparrow} + R_{2\downarrow}) + R_{2\uparrow}R_{2\downarrow}(R_{1\uparrow} + R_{1\downarrow})]^2},$$
(3)

For simplicity we can directly consider a DBMTJ as two SBMTJs in series and Eq.(3) can become to $F_{incoherent} = 1 - \frac{2R_1 R_2}{(R_1 + R_2)^2}$,where $R_i = (R_{i\uparrow}R_{i\downarrow})/(R_{i\uparrow} + R_{i\downarrow})$ is the resistance of the i-th barrier.

The spin relaxation length is limited by spin-orbital or spin-spin scattering from defects or impurities and

scattering by phonons and magnons[30,31]. Scattering by phonons and magnons decreases with decreasing temperature. In this case, the tunneling process could change from incoherent limit to coherent limit as temperature decreases from high temperature to low. Therefore F will change as the spin relaxation length changes at different temperature.

As in previous work[20], the following parameters are introduced: $\alpha = R_{2\uparrow}^0/R_{1\uparrow}^0$, $\beta_1 = R_{1\downarrow}^0/R_{1\uparrow}^0$, and $\beta_2 = R_{2\downarrow}^0/R_{2\uparrow}^0$, where $R_{i\uparrow(\downarrow)}^0$ is the resistance of i-th barrier for spin majority(minority) electrons in the state with parallel magnetizations on both sides. If we choose $\alpha = 0.25, \beta_1 = 1.1, \beta_2 = 100$, for the AP2 state: $F_{incoherent} = 0.56$ and $F_{coherent} = 0.69$, which is compatible with our results(0.55 at 296 K and 0.71 at 20 K). These parameters are selected specifically for the sample asymmetric structure. The spin diffusion length of $Co_{40}Fe_{40}B_{20}$ and $Co_{50}Fe_{50}$ was found to be 4.5 nm and 9 nm at 4 K[32,33] which is larger than the thickness of the 3 nm middle layer in our sample. It seems possible that the tunneling reaches coherent limit at 20 K in our sample. For AP1, F also increases at low temperature and approaches 1 below 78 K. This is caused by the strongly asymmetric structure of our device. The Fano factor will approach 1 when $\beta_2 \gg \beta_1$ no mater it is coherent or incoherent tunneling.

Shot noise was also measured in single barrier MTJs, where F was close to 1 and no temperature dependence was found. Results are shown in appendix C.

IV. CONCLUSION

In conclusion, we measured shot noise at room temperature in a high-frequency bandwidth(2.1-2.5 MHz) and find that shot noise in the asymmetric DBMTJ shows temperature and magnetic state dependence. At a given temperature, the Fano factor is much larger in high resistance AP1 state than in other four states. It increases as temperature decreases from room temperature to low temperature for all magnetic states. We interpret our findings with larger spin relaxation length in the middle ferromagnetic layer at lower temperatures by using sequential tunneling model.

V. ACKNOWLEDGMENTS

APPENDIX A: TYPICAL SPECTRUM

Figure 6 shows typical noise spectra of $AP1^r$ state at room temperature for bias current of 40 uA(green) and 510 uA(red). We can select a suitable frequency range with flat noise power to get accurate white noise power. There is extra noise from amplifier AU1447 in the range of 0.1 kHz-4 kHz which is the same for both current values. Below 100 kHz, the fast increase of the noise could be due to 1/f noise. The peak between 5 MHz and 15 MHz is extra noise from ground loop. The damping at high frequency (>15 MHz) is caused by a low pass filter to avoid frequency aliasing[34]. 2.1-2.5 MHz is used to measure shot noise and is shown in insert. Obviously, 1/f noise is much smaller than shot noise at this frequency range. And shot noise increases with increasing bias current.

APPENDIX B: ANOTHER DBMTJ SAMPLE

Similar results are shown in Fig. 7 for another DBMTJ sample(DB2) with lower TMR (150%). Noise is again measured at 2.1-2.5 MHz and differential resistance is used to calculate current noise. Fano factor in this sample also shows temperature and magnetic state dependence. Fano factor of the AP1 state is larger than AP2 state, and it increases with temperature decreasing.
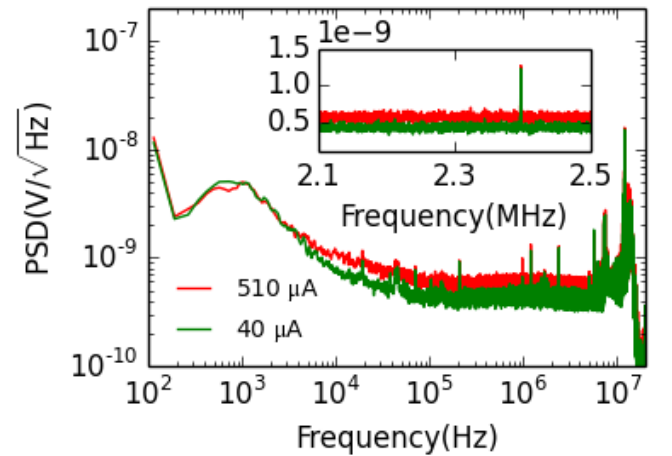

FIG. 6. (color online)Typical spectrum measured of $AP1^r$ state at room temperature for 40 uA(green) and 510 uA(red) bias current. The insert shows the frequency used to measure shot noise.
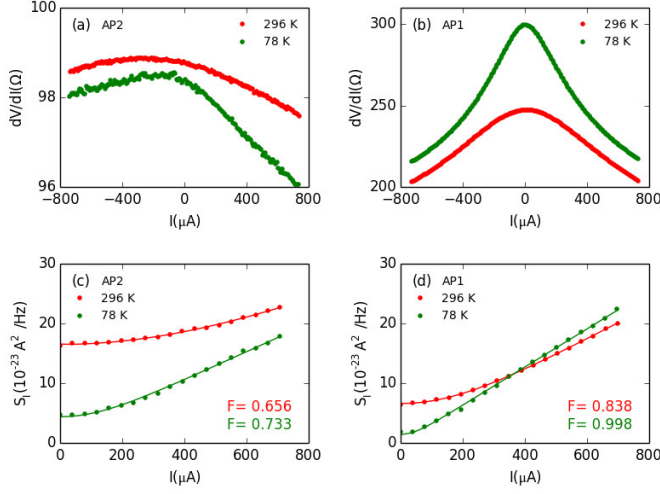
FIG. 7. (color online)Similar temperature and resistance dependence of Fano factor in another DBMTJ sample(DB2). (a) and (b) show differential resistance of AP2 and AP1 state. Bias dependence of noise power S_I is shown for (a)AP2 state and (b)AP1 state. For both states, Fano factor at AP1 state is larger than AP2 state.
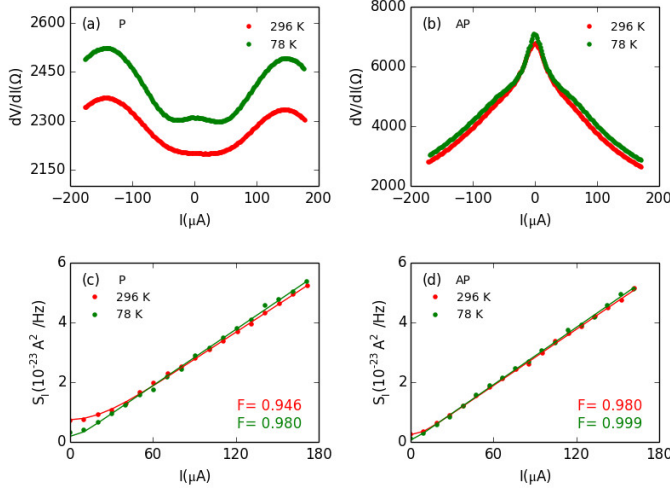

FIG. 8. (color online)Differential resistance and noise in a single barrier MTJ. (a) and (b) show differential resistance for P and AP state at two temperatures. Bias dependence of noise power S_I at different temperatures is measured for (c)P state and (d)AP state. Fano factor does not show obvious temperatures and field dependence in single barrier MTJ.

APPENDIX C: SINGLE BARRIER MTJ

Noise was measured in single-barrier MTJ sample with nearly 300% TMR. Results are shown in Fig. 8. The differential resistance for P and AP state are shown in

Fig. 8 (a) and (b). (c) and (d) show the bias dependence of noise power at two temperatures. The Fano factor does not show an obvious temperature or magnetic state dependence in single-barrier MTJ case.

APPENDIX D: VOLTAGE DEPENDENCE

The voltage dependence of resistance could be more informative especially for studying the spin transport property. Figure 9 shows the voltage dependence of differential resistance for AP2 and AP1 states at three typical temperatures.

APPENDIX E: CALIBRATION OF AMPLIFIER

The current noise power measured by AU1447 is $S_{measured} = \frac{R_{sample}^2}{(R_{sample}+50)^2}S_I$, where R_{sample} is the resistance of sample and S_I is the current noise of sample. When R_{sample} is much larger than the 50 Ω impedance, the current noise measured will approach the current noise of sample. In this work, current noise of sample is calculated by $S_I = \frac{(R_{sample}+50)^2}{R_{sample}^2}S_{measrued}$ to get accurate Fano factor even though R_{sample} is much larger than 50.

The effective gain of amplifier is calibrated by a signal generator (Agilent 33521A) at three temperatures (296 K, 78 K, 20 K) below 3 MHz. A standard sine wave current excitation ($I = 10\mu A$) is applied to the junction. The the voltage measured should be $V = \frac{R_{sample}}{R_{sample}+50} \times I \times 50 \times Gain$, where $Gain$ is the effective gain of the amplifier. Effective gain is calibrated by this way. Not only DBMTJs but also different resistors (200 Ω, 500 Ω, 1 $k\Omega$ and 10 $k\Omega$) and SBMTJs are used as samples to complete this calibration. The effective gain does not change with temperature and R_{sample} below 3 MHz for all samples.
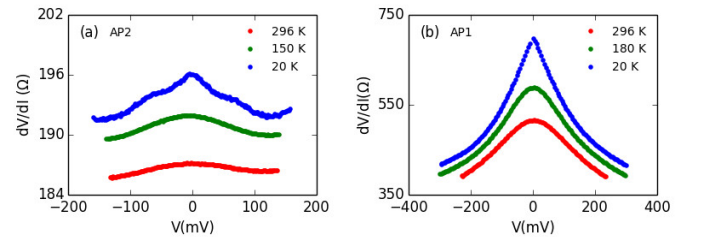

FIG. 9. (color online)(a) and (b) show voltage dependence of differential resistance for AP2 and AP1 state at three typical temperatures.

* jiasenniu@pku.edu.cn

[1] J. S. Moodera, L. R. Kinder, T. M. Wong, and R. Meservey, Phys. Rev. Lett. **74**, 3273 (1995).

[2] T. Miyazaki and N. Tezuka, Journal of Magnetism and Magnetic Materials **139**, L231 (1995).

[3] W. H. Butler, X.-G. Zhang, T. C. Schulthess, and J. M. MacLaren, Phys. Rev. B **63**, 054416 (2001).

[4] J. Mathon and A. Umerski, Phys. Rev. B **63**, 220403 (2001).

[5] S. S. P. Parkin, C. Kaiser, A. Panchula, A. Panchula, P. M. Rice, B. Hughes, M. Samant, and S.-H. Yang, Nat Mater **3**, 862 (2004).

[6] S. Yuasa, T. Nagahama, A. Fukushima, Y. Suzuki, and K. Ando, Nat Mater **3**, 868 (2004).

[7] J. Faure-Vincent, C. Tiusan, E. Jouguelet, F. Canet, M. Sajieddine, C. Bellouard, E. Popova, M. Hehn, F. Montaigne, and A. Schuhl, Applied Physics Letters **82**, 4507 (2003), https://doi.org/10.1063/1.1586785.

[8] M. Bowen, V. Cros, F. Petroff, A. Fert, C. M. Boubeta, J. L. Costa-Kramer, J. V. Anguita, A. Cebollada, F. Briones, J. M. de Teresa, L. Morellon, M. R. Ibarra, F. Guell, F. Peiro, and A. Cornet, Applied Physics Letters **79**, 1655 (2001), https://doi.org/10.1063/1.1404125.

[9] C. Tiusan, M. Sicot, M. Hehn, C. Belouard, S. Andrieu, F. Montaigne, and A. Schuhl, Applied Physics Letters **88**, 062512 (2006), https://doi.org/10.1063/1.2172717.

[10] S. Yuasa and D. D. Djayaprawira, Journal of Physics D: Applied Physics **40**, R337 (2007).

[11] T. Nozaki, N. Tezuka, and K. Inomata, Phys. Rev. Lett. **96**, 027208 (2006).

[12] Y. Wang, Z.-Y. Lu, X.-G. Zhang, and X. F. Han, Phys. Rev. Lett. **97**, 087210 (2006).

[13] C. Tiusan, F. Greullet, M. Hehn, F. Montaigne, S. Andrieu, and A. Schuhl, Journal of Physics: Condensed Matter **19**, 165201 (2007).

[14] D. L. Li, J. F. Feng, G. Q. Yu, P. Guo, J. Y. Chen, H. X. Wei, X. F. Han, and J. M. D. Coey, Journal of Applied Physics **114**, 213909 (2013).

[15] B. S. Tao, H. X. Yang, Y. L. Zuo, X. Devaux, G. Lengaigne, M. Hehn, D. Lacour, S. Andrieu, M. Chshiev, T. Hauet, F. Montaigne, S. Mangin, X. F. Han, and Y. Lu, Phys. Rev. Lett. **115**, 157204 (2015).

[16] G. Q. Yu, Z. Diao, J. F. Feng, H. Kurt, X. F. Han, and J. M. D. Coey, Applied Physics Letters **98**, 112504 (2011).

[17] G. Feng, S. van Dijken, J. F. Feng, J. M. D. Coey, T. Leo, and D. J. Smith, Journal of Applied Physics **105**, 033916 (2009).

[18] R. Guerrero, D. Herranz, F. G. Aliev, F. Greullet, C. Tiusan, M. Hehn, and F. Montaigne, Applied Physics Letters **91**, 132504 (2007), https://doi.org/10.1063/1.2793619.

[19] R. Guerrero, F. G. Aliev, Y. Tserkovnyak, T. S. Santos, and J. S. Moodera, Phys. Rev. Lett. **97**, 266602 (2006).

[20] J. Cascales, D. Herranz, F. Aliev, T. Szczepański, V. Dugaev, J. Barnaś, A. Duluard, M. Hehn, and C. Tiusan, Phys. Rev. Lett. **109**, 066601 (2012).

[21] Y. P. Li, A. Zaslavsky, D. C. Tsui, M. Santos, and M. Shayegan, Phys. Rev. B **41**, 8388 (1990).

[22] A. GOKCE, R. STEARRETT, E. R. NOWAK, and C. NORDMAN, Fluctuation and Noise Letters **10**, 381 (2011), http://www.worldscientific.com/doi/pdf/10.1142/S0219477511000648.

[23] B. R. Bułka, J. Martinek, G. Michałek, and J. Barnaś, Phys. Rev. B **60**, 12246 (1999).

[24] Y. Blanter and M. Buttiker, Physics Reports **336**, 1 (2000).

[25] K. Sekiguchi, T. Arakawa, Y. Yamauchi, K. Chida, M. Yamada, H. Takahashi, D. Chiba, K. Kobayashi, and T. Ono, Applied Physics Letters **96**, 252504 (2010), http://dx.doi.org/10.1063/1.3456548.

[26] T. Szczepański, V. K. Dugaev, J. Barnaś, J. P. Cascales, and F. G. Aliev, Phys. Rev. B **87**, 155406 (2013).

[27] L. Liu, J. Niu, H. Guo, J. Wei, D. L. Li, J. F. Feng, X. F. Han, J. M. D. Coey, and X.-G. Zhang, Phys. Rev. B **93**, 180401 (2016).

[28] G. Hui-Qiang, T. Wei-Yue, L. Liang, W. Jian, L. Da-Lai, F. Jia-Feng, and H. Xiu-Feng, Chinese Physics B **24**, 078504 (2015).

[29] P. Zhou, W. J. Hardy, K. Watanabe, T. Taniguchi, and D. Natelson, Applied Physics Letters **110**, 133106 (2017), https://doi.org/10.1063/1.4978693.

[30] A. Brataas, Y. V. Nazarov, J. Inoue, and G. E. W. Bauer, Phys. Rev. B **59**, 93 (1999).

[31] J. Bass and W. P. P. Jr, Journal of Physics: Condensed Matter **19**, 183201 (2007).

[32] C. Ahn, K.-H. Shin, and W. P. P. Jr., Applied Physics Letters **92**, 102509 (2008), http://dx.doi.org/10.1063/1.2891065.

[33] C. Ahn, K.-H. Shin, R. Loloee, J. Bass, and W. P. P. Jr., Journal of Applied Physics **108**, 023908 (2010), http://dx.doi.org/10.1063/1.3436584.

[34] L. DiCarlo, Y. Zhang, D. T. McClure, C. M. Marcus, L. N. Pfeiffer, and K. W. West, Review of Scientific Instruments **77**, 073906 (2006), http://dx.doi.org/10.1063/1.2221541.